

R-mode Stability of GW190814's Secondary Component as a Supermassive and Superfast Pulsar

XIA ZHOU,¹ ANG LI,² AND BAO-AN LI³

¹*Xinjiang Astronomical Observatory, Chinese Academy of Sciences, Urumqi, Xinjiang 830011, China*

²*Department of Astronomy, Xiamen University, Xiamen, Fujian 361005, China*

³*Department of Physics and Astronomy, Texas A&M University-Commerce, Commerce, TX 75429, USA*

(Dated: February 11, 2021)

ABSTRACT

The nature of GW190814's secondary component m_2 of mass $(2.50 - 2.67) M_\odot$ in the mass gap between the currently known maximum mass of neutron stars and the minimum mass of black holes is currently under hot debate. Among the many possibilities proposed in the literature, the m_2 was suggested as a superfast pulsar while its r-mode stability against the run-away gravitational radiation through the Chandrasekhar-Friedman-Schutz mechanism is still unknown. Using those fulfilling all currently known astrophysical and nuclear physics constraints among a sample of 33 unified equation of states (EOSs) constructed previously by Fortin *et al.* (2016) using the same nuclear interactions from the crust to the core consistently, we compare the minimum frequency required for the m_2 to rotationally sustain a mass higher than $2.50 M_\odot$ with the critical frequency above which the r-mode instability occurs. We use two extreme damping models assuming the crust is either perfectly rigid or elastic. Using the stability of 19 observed low-mass x-ray binaries as an indication that the rigid crust damping of the r-mode dominates within the models studied, we find that the m_2 is r-mode stable while rotating with a frequency higher than 870.2 Hz (0.744 times its Kepler frequency of 1169.6 Hz) as long as its temperate is lower than about $3.9 \times 10^7 K$, further supporting the proposal that GW190814's secondary component is a supermassive and superfast pulsar.

Keywords: Pulsars (1306); Neutron stars (1108)

1. INTRODUCTION

The recent discovery by the LIGO/Virgo Collaborations that the compact binary merger GW190814 has a secondary component m_2 with mass $(2.50 - 2.67) M_\odot$ (Abbott *et al.* 2020) at 90% credible level has generated much interest in the astrophysics community. As the m_2 is in the mass gap between the currently known maximum mass of neutron stars and the minimum mass of black holes, its nature has significant ramifications on many interesting issues in astrophysics and cosmology. Many possibilities regarding its nature and formation path have been proposed very recently in the literature; see, e.g., Roupas *et al.* (2020); Biswas *et al.* (2020); Bombaci *et al.* (2020) among the latest reports and references therein.

Since the maximum mass M_{TOV} of non-rotating neutron stars is predicted to be about $2.4 M_\odot$ on the causality surface with the equation of state (EOSs) satisfying all known constraints (e.g., Zhang & Li 2019; Li *et al.* 2020) and it is well known that the centrifugal force in neutron stars rotating at Kepler frequencies can increase their maximum masses by about 20% with respect to the M_{TOV} , the mass of m_2 is well within reach with the rotational support. Indeed, this possibility is among the first one considered. However, the conclusions have been diverse mainly because of the different nuclear EOSs used (see e.g., Abbott *et al.* 2020; Biswas *et al.* 2020; Dexheimer *et al.* 2020; Godzieba *et al.* 2020; Huang *et al.* 2020; Tews *et al.* 2020; Most *et al.* 2020; Zhang & Li 2020; Zhang & Mann 2020). Among the conclusions supporting the m_2 as a superfast pulsar, Most *et al.* (2020) found that m_2 has a rotation frequency of 1210 Hz assuming it has a typical neutron star radius of 12.5 km and a $M_{\text{TOV}}=2.08 M_\odot$. In another study by Zhang & Li (2020), the m_2 was found

to have a rotation frequency of 971 Hz using a EOS leading to an equatorial radius of 11.9 km for m_2 and a $M_{\text{TOV}}=2.39 M_{\odot}$. More recently, Biswas et al. (2020) derived a minimum frequency of 1143_{-155}^{+194} Hz and an equatorial radius $R_e = 15.7_{-1.7}^{+1.0}$ km for m_2 at 90% confidence level assuming a $M_{\text{TOV}}=2.14 M_{\odot}$ which is the mass of MSR J0740+6620 (Cromartie et al. 2020). The minimum frequencies found for m_2 in these studies are significantly higher than the fastest known pulsar PSR J1748-2446ad with a frequency of 716 Hz (Hessels et al. 2006), thus making GW190814's secondary the most massive and fastest known pulsar if confirmed.

While the LIGO/Virgo Collaborations tightly constrained the primary spin of GW190814, the spin of its secondary m_2 remains unconstrained (Abbott et al. 2020). Thus, the possibility for the m_2 as a superfast pulsar is neither confirmed nor ruled out observationally. However, an outstanding question critical for the m_2 to be a superfast pulsar remains to be answered. Namely, it is unknown if the m_2 with the required minimum frequencies are stable against the well-known r-mode instability leading to the exponential growth of gravitational radiation. As it was pointed out already in Zhang & Li (2020); Biswas et al. (2020), for the m_2 to be a supermassive and superfast pulsar, its rotational instabilities would have to be suppressed, otherwise, it is more likely to be a black hole instead.

In this work, we examine the r-mode instability of m_2 using well established EOSs satisfying all currently known constraints within the r-mode formalisms established by Lindblom et al. (1998, 2000). While a multitude of damping mechanisms exist, an instability can develop only if its growth is faster than its strongest damping mechanism (Biswas et al. 2020). It is known that a rigid crust provides the strongest r-mode damping, and it can well explain the stability of all observed low-mass x-ray binaries (LMXBs) (e.g., Ho et al. 2011; Haskell et al. 2012). Using this damping mechanism, we found that the m_2 can be r-mode stable as long as its temperature is sufficiently low, e.g., lower than about $3.9 \times 10^7 K$ for the m_2 rotating at 1169.6 Hz (0.744 times its Kepler frequency). Since this temperature is about an order of magnitude higher than that of some known old neutron stars (see, e.g., Wijngaarden et al. 2019), the r-mode instability should not be a concern for the m_2 as a supermassive and superfast pulsar within the theoretical framework and models considered.

The r-mode instability (Andersson 1998; Friedman & Morsink 1998; Andersson & Kokkotas 1998; Ho & Lai 2000) can trigger the exponential growth of gravitational wave (GW) emission in rapidly rotating neutron stars through the Chandrasekhar-Friedman-Schutz

mechanism (Chandrasekhar 1970; Friedman & Schutz 1978) if the GW growth rate is faster than its damping rate. Over the past two decades, significant efforts have been devoted to better understanding the r-mode instability and its damping mechanisms with many interesting findings (see, e.g., Madsen 2000; Sá 2004; Sá & Tomé 2005; Andersson et al. 2010; Haskell & Andersson 2010; Yang et al. 2011; Wen et al. 2012; Vidaña 2012; Haskell et al. 2012; Alford & Schwenzer 2014a,b; Idrisy et al. 2015; Moustakidis 2015; Dai et al. 2016; Papazoglou & Moustakidis 2016; Ofengeim et al. 2019; Wang et al. 2019; Krüger & Kokkotas 2020). In particular, it was found that the r-mode instability window (a region in the spin frequency versus temperature plane) in which the r-mode is unstable depends sensitively on the EOS of neutron-rich matter, especially its symmetry energy term which encodes the information about the energy cost to make nuclear matter more neutron-rich. It depends even more sensitively on the poorly known properties of neutron star crust, especially whether it is rigid or elastic (see more discussions in recent reviews, e.g., Andersson & Kokkotas 2001; Haskell 2015; Andersson 2017; Kokkotas & Schwenzer 2016). To realize the goal of this work, it is thus critical to use unified EOSs for neutron stars not only satisfying all currently known constraints from both nuclear physics and astrophysics but also describing the crust, crust-core transition, and the core consistently based on the same nuclear interactions within the same nuclear many-body theories. Moreover, it is important to limit the uncertain r-mode damping mechanisms as much as possible and to identify the strongest one using existing astrophysical observations.

For the purposes outlined above, we describe in the next section how we selected the unified EOSs satisfying the conditions mentioned above. In Section 3, we compare 19 observed LMXBs with known frequencies and temperatures with the r-mode instabilities boundaries calculated with the selected unified EOSs assuming the crust is either perfectly rigid or elastic. As expected, the stability of the 19 LMXBs prefers the perfectly rigid crust. Assuming the same damping mechanism is at work in other neutron stars, we infer in Section 4 the maximum temperature of m_2 by comparing the minimum frequency it must have to sustain rotationally a mass of $2.50 M_{\odot}$ with the maximum frequency it can have before the r-mode instability occurs. We then summarize our work in Sec. 5.

2. UNIFIED EOS FOR NEUTRON STARS

Various EOSs for neutron stars have been used in the literature. Often, they are constructed from combining

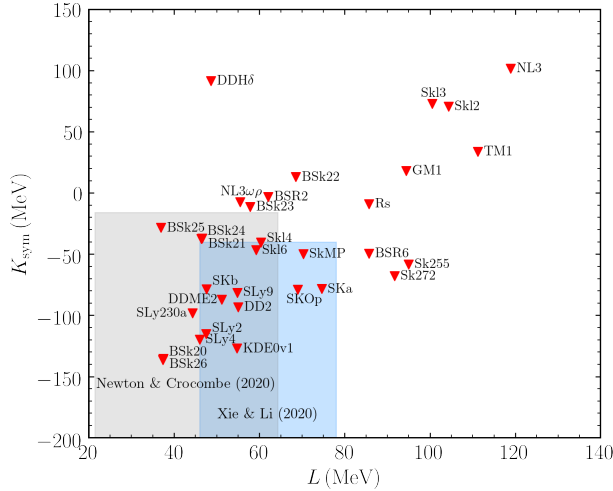


Figure 1. K_{sym} parameter as a function of L for the 33 unified neutron star EOSs from Fortin et al. (2016), together with two recent constraints, to the 68% confidence level, on the slope L and curvature K_{sym} of the symmetry energy at saturation (Newton & Crocombe 2020; Xie & Li 2020). Note that the 95% confidence boundaries shown in Newton & Crocombe (2020) are rescaled to the 68% credible ranges here for a comparison. Only 7 EOSs: DD2, DDME2, KDE0v1, SKb, SkI6, SLy2, and SLy9 fulfill both constraints.

the EOSs for the core and crust calculated using different models and/or interactions. For most purposes, these EOSs are perfectly fine. As we discussed above, for the purpose of this work, it is advantageous to use the EOSs with the crust, crust-core transition, and core all calculated using the same nuclear interaction. We thus adopt the 33 unified EOSs derived by Fortin et al. (2016) within the Skyrme Hartree-Fock and the Relativistic mean-field models for the core and the Thomas-Fermi model for the crust using the same interactions. Because new progress has been made in constraining the EOS since these 33 EOSs were derived, we shall first filter them through the following three tests: (1) satisfying new constraints on the density dependence of nuclear symmetry energy from analyzing both nuclear experiments and astrophysical observations especially the radii and tidal deformability of neutron stars (Newton & Crocombe 2020; Xie & Li 2020), (2) being stiff enough to support the presently known maximum mass of neutron stars, i.e., the $M = 2.14_{-0.09}^{+0.10} M_{\odot}$ (68% confidence level) of MSP J0740+6620 (Cromartie et al. 2020), (3) be consistent with the simultaneous mass and radius measurements by NICER for PSR J0030+0451 (Miller et al. 2019; Raaijmakers et al. 2019; Riley et al. 2019).

The nuclear symmetry energy is well-known to have significant effects on the structure of neutron stars (Lattimer & Prakash 2000; Steiner et al. 2005; Li et al. 2019), including the crust-core transition, the crust thickness, as well as the composition of the star. For a comprehen-

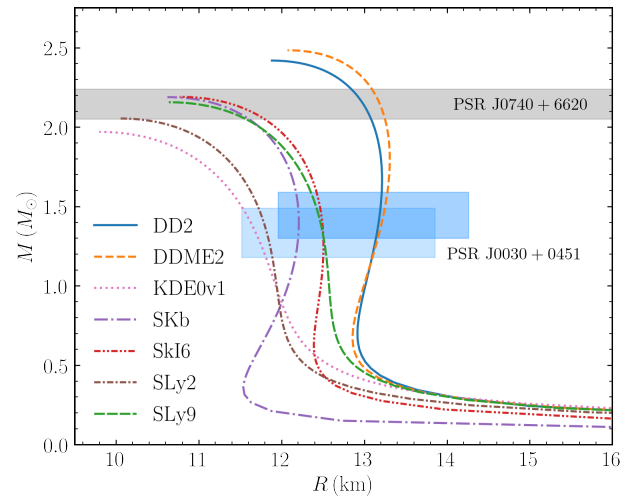


Figure 2. Mass-radius relations of neutron stars using the 6 EOSs from Fig. 1 satisfying the latest constraints on L and K_{sym} . The astrophysical constraining bands on the maximum mass (Cromartie et al. 2020) and the mass-radius correlations for PSR J0030+0451 from NICER (Miller et al. 2019; Raaijmakers et al. 2019; Riley et al. 2019) are shown for comparisons.

sive review on nuclear symmetry energy and its astrophysical effects, we refer the reader to Li et al. (2014). It is defined as

$$E_{\text{sym}}(n) = \frac{1}{2} \frac{\partial^2 E(n, \beta)}{\partial \beta^2} \Big|_{\beta=0}, \quad (1)$$

where $E(n, \beta)$ is the binding energy of neutron-rich matter as a function of density n and isospin asymmetry $\beta = (n_n - n_p)/n$. The $E_{\text{sym}}(n)$ can be characterized by using its slope L and curvature K_{sym} at the nuclear saturation density n_0 defined as

$$L = 3n_0 [\partial E_{\text{sym}}(n) / \partial n] \Big|_{n=n_0}, \quad (2)$$

$$K_{\text{sym}} = 9n_0^2 [\partial^2 E_{\text{sym}}(n) / \partial n^2] \Big|_{n=n_0}. \quad (3)$$

It was shown earlier that both the L and especially K_{sym} as well as their correlation affect the crust-core transition density and pressure significantly (e.g., Xu et al. 2009; Vidaña et al. 2009; Zhang et al. 2018; Providência et al. 2019; Li & Magno 2020). They also affect the EOS and especially the composition of the core (Lattimer et al. 1991). Fortunately, some significant progresses have been made recently in experimentally constraining the slope parameter L (Li & Han 2013; Baldo & Burgio 2016; Oertel et al. 2017), while the curvature K_{sym} is still much less constrained. In particular, a recent Bayesian analysis of the radii and tidal deformations of canonical neutron stars (Xie & Li 2020) inferred the most probable values of $L = 66_{-20}^{+12}$ MeV and $K_{\text{sym}} = -120_{-100}^{+80}$ MeV at 68% confidence level. In another Bayesian analysis by Newton & Crocombe

(2020) using combined data of neutron skin in ^{48}Ca , ^{208}Pb and tin isotopes as well as the best theoretical information about the EOS of pure neutron matter from *ab initio* microscopic nuclear many-body theories, the most probable values of L and K_{sym} were found to be $L = 40_{-26}^{+34}$ MeV and $K_{\text{sym}} = -209_{-182}^{+270}$ MeV, respectively, at 95% confidence level.

Shown in Fig. 1 are the two constraints on L and K_{sym} in comparison with predictions of the 33 unified EOSs from Fortin et al. (2016). It is seen that only 7 of them fall into the overlapping area of the two latest constraints (Newton & Crocombe 2020; Xie & Li 2020). We further test them against the latest astrophysical observations in Fig. 2. It is seen that the KDE0v1 EOS is further excluded by the mass measurement of MSP J0740+6620, to the 68.3% credibility interval, while the remaining 6 EOSs can support a maximum mass of about $2.14 M_{\odot}$ (Cromartie et al. 2020) and satisfy the mass-radius constraints from NICER (Miller et al. 2019; Riley et al. 2019). Thus, we will only use these 6 unified EOSs in our further studies in the following.

3. R-MODE INSTABILITY IN NEUTRON STARS

All rotating neutron stars are generically r-mode unstable due to the emission of gravitational waves. However, there are several possible damping mechanisms preventing the r-mode oscillation from growing exponentially. Here we adopt two extreme damping models assuming the crust is either rigid or elastic. For easy of discussions, in the following, we first recall briefly some of the basic definitions and formulas most relevant for our study about the r-mode instability of m_2 . We refer the reader to the original papers for more details.

3.1. Time scales of r-mode growth and damping

Whether the r-mode oscillation can grow exponentially or not depends on the competition between the growth rate of gravitational wave emission and the r-mode damping rate (mainly due to viscosity). Thus, the r-mode instability boundary is determined by setting the damping τ_{diss} and driving τ_{gw} timescales equal to each other (Andersson & Kokkotas 2001), i.e., by solving for the zeros of

$$-\frac{1}{2\dot{E}} \left(\frac{d\tilde{E}}{dt} \right) = \frac{1}{\tau_{\text{gw}}(\nu)} + \sum \frac{1}{\tau_{\text{diss}}(\nu, T)} = 0, \quad (4)$$

where \tilde{E} is the total energy of an r-mode oscillation. It is known that the shear viscosity dominates the energy dissipation for temperatures around 10^8 K, while at higher temperatures (of the order of 10^{10} K) the bulk viscosity becomes important (Andersson & Kokkotas 2001). Since all the observed LMXBs have temperatures around 10^8 K and the old neutron stars are

cooler, in the present study we consider only the shear viscosity resulting from both neutron-neutron (nn) and electron-electron (ee) scatterings. We adopt the following parameterizations for the two viscosities as functions of temperature T (Flowers & Itoh 1979; Cutler & Lindblom 1987; Shternin & Yakovlev 2008),

$$\eta_{nn}(r) = 347[\rho(r)]^{9/4} T^{-2} \quad (\text{g cm}^{-1}\text{s}^{-1}), \quad (5)$$

$$\eta_{ee}(r) = 6 \times 10^6 [\rho(r)]^2 T^{-2} \quad (\text{g cm}^{-1}\text{s}^{-1}), \quad (6)$$

where $\rho(r)$ is the mass density profile of the star.

The crust is expected to play an important role in determining the r-mode stability of neutron stars. Here we consider two extreme cases. Assume the crust is perfectly rigid (i.e., the ‘‘slippage’’ factor $S = 1$), so the fluid motion associated with the r-mode would be significantly damped at the crust-core boundary, the τ_{gw} is given by (Lindblom et al. 2000),

$$\frac{1}{\tau_{\text{gw}}^c} = -\frac{32\pi G \Omega^{2l+2}}{c^{2l+3}} \frac{(l-1)^{2l}}{[(2l+1)!!]^2} \left(\frac{l+2}{l+1} \right)^{2l+2} \times \int_0^{R_c} \rho(r) r^{2l+2} dr, \quad (7)$$

where G is the gravitational constant, $\Omega = 2\pi\nu$ is the angular velocity of the star, c is the speed of light and R_c is the stellar radius at the crust-core transition mass density ρ_c . While the τ_{diss} can be evaluated from (Lindblom et al. 2000),

$$\tau_{\eta}^c = \frac{1}{2\Omega} \frac{2^{l+3/2}(l+1)!}{l(2l+1)!!\mathcal{C}_l} \sqrt{\frac{2\Omega R_c^2 \rho_c}{\eta_c}} \int_0^{R_c} \frac{\rho}{\rho_c} \left(\frac{r}{R_c} \right)^{2l+2} \frac{dr}{R_c}, \quad (8)$$

where η_c is the viscosity at the crust-core transition density. Following Lindblom et al. (1998), we only consider the lowest order contribution of the multipole moment ($l = 2$), with $\mathcal{C}_2 = 0.80411$ (Rieutord 2001).

In the other extreme case neglecting the crustal damping, or the crust is regarded as extremely elastic [i.e., the ‘‘slippage’’ factor $S \rightarrow 0$ (see e.g., Glampedakis & Andersson 2006)], the crust will also participate in the oscillation. In this case, the τ_{gw} is given by (Lindblom et al. 1998),

$$\frac{1}{\tau_{\text{gw}}} = -\frac{32\pi G \Omega^{2l+2}}{c^{2l+3}} \frac{(l-1)^{2l}}{[(2l+1)!!]^2} \left(\frac{l+2}{l+1} \right)^{2l+2} \times \int_0^R \rho(r) r^{2l+2} dr. \quad (9)$$

While the τ_{η} is written as (e.g., Vidaña 2012),

$$\frac{1}{\tau_{\eta}} = (l-1)(2l+1) \left(\int_0^R \rho(r) r^{2l+2} dr \right)^{-1} \times \int_0^R \eta(r) r^{2l} dr. \quad (10)$$

The actual neutron star crust should have some elasticity, therefore by calculating the r-mode boundary in

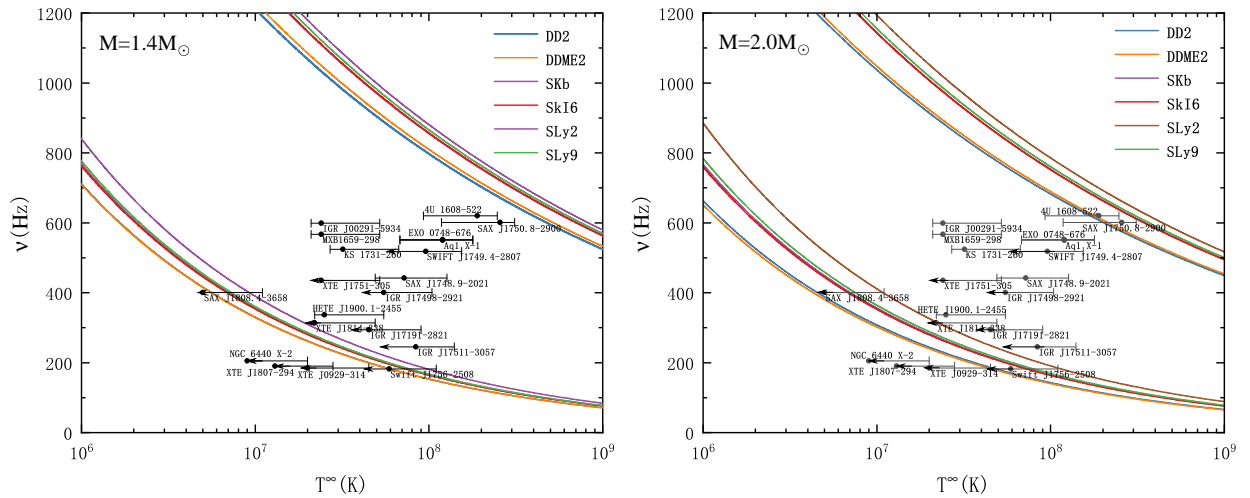


Figure 3. Locations of LMXBs in the frequency-temperature plane and lower bounds ν_{crit} of the r-mode instability windows for $1.4 M_{\odot}$ (left) and $2.0 M_{\odot}$ (right) neutron stars with 6 selected unified EOSs. The upper (lower) group of lines are calculated with rigid (elastic) crusts. The observational data and internal redshifted temperatures ($T^{\infty} = T\sqrt{1 - 2GM/Rc^2}$) on neutron stars in LMXBs are taken from [Gusakov et al. \(2014\)](#); [Chugunov et al. \(2017\)](#), with the error bars due to the uncertainty in the composition of the envelope (see detail in [Gusakov et al. 2014](#); [Chugunov et al. 2017](#)).

the two extreme cases: Eqs. (7)-(8) (where a rigid crust is considered) and Eqs. (9)-(10) (where no crustal damping is included), we may estimate the uncertainty due to the crustal modelling. Moreover, confronting the theoretical results with the observations of neutron stars' frequency and temperatures in LMXBs, we may get some hints about which damping mechanism dominates.

3.2. Lower boundaries of r-mode instability windows

From Eq. (4), for each star at a given temperature, one can find its critical frequency ν_{crit} above which the star becomes unstable against the running-off of gravitational radiation, by setting $1/\tau_{\text{gw}}(\nu_{\text{crit}}) + 1/\tau_{\eta}(\nu_{\text{crit}}, T) = 0$. The ν_{crit} serves as an upper limit of stable pulsars' frequencies for a given temperature. The region above this boundary in the frequency-temperature plane is the so-called r-mode instability window. In the following, we examine the r-mode instability boundaries with the 6 selected EOSs with respect to the locations of the 19 LMXBs. Since the masses of the neutron stars in these LMXBs are not measured accurately, the calculations are done for both canonical ($M = 1.4 M_{\odot}$) and massive ($M = 2.0 M_{\odot}$) neutron stars.

Our results are shown in Fig. 3 for both cases assuming a perfectly rigid crust (upper groups of lines) or an elastic one (lower group of lines). Several interesting observations can be made:

- The r-mode instability boundary depends most sensitively on the crust's elasticity while effects of the EOS and neutron star mass are appreciable. Most importantly, for the present study, the rigid crust provides the strongest damping.

- The damping mechanism with a perfectly rigid crust can accommodate all neutron stars in the 19 LMXBs, while the one with an elastic crust can only accommodate a few slowly-rotating neutron stars, such as NGC 6440 X-2, XTE J1807-294, and XTE J0929-314.
- The r-mode instability boundaries are sensitive to the EOS especially the L parameter (see e.g., [Wen et al. 2012](#)), but the effects shown here are much less than previously reported in the literature mainly because the 6 unified EOSs used here are much more stringently constrained compared to those used before. Nevertheless, one can still clearly see that the L parameter (shown in Fig. 1) can not be very large, e.g., smaller than ~ 60 MeV if LMXB neutron stars are massive (e.g., $M = 2.0 M_{\odot}$), to ensure the rapidly-rotating neutron stars in, e.g., 4U 1608-522 and SAX J1705.8-2900, stay r-mode stable.
- Comparing the results for $1.4 M_{\odot}$ and $2.0 M_{\odot}$ neutron stars, we see that the r-mode instability window is generally broader for the latter in agreement with earlier findings (e.g., [Vidaña 2012](#)), especially in the case with the rigid crust. Moreover, the uncertainty band due to the EOS is relatively wider for neutron stars of mass $2.0 M_{\odot}$, due to the more significant diversity of the EOS at higher densities reached.

Since the Kepler frequency ν_K is the absolute upper limit of spin frequencies of all stars with a given mass, it is interesting and informative to examine the reduced

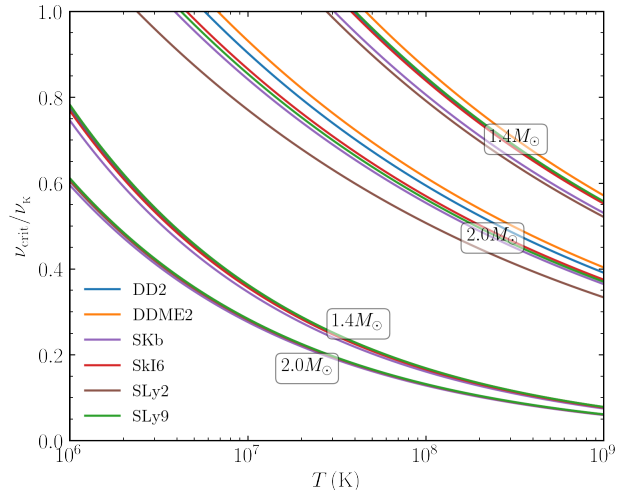


Figure 4. Temperature dependence of the reduced critical frequency $\nu_{\text{crit}}/\nu_{\text{K}}$ for $M = 1.4 M_{\odot}$ and $M = 2.0 M_{\odot}$ neutron stars with rigid (upper groups of lines) or elastic crusts (lower groups of lines).

critical frequency $\nu_{\text{crit}}/\nu_{\text{K}}$ as functions of the temperature T for both $1.4 M_{\odot}$ and $2.0 M_{\odot}$ neutron stars. Our results for $\nu_{\text{crit}}/\nu_{\text{K}}$ are shown in Fig. 4. Compared to the un-scaled results shown in Fig. 3, it is seen that the r-mode instability boundaries of the reduced frequency are more sensitive to the neutron star mass with both rigid and elastic crusts. This is because the ν_{K} is proportional to the square root of the average density of neutron stars (Andersson & Kokkotas 2001). The average density depends on the mass; thus, the reduced frequency becomes more sensitive to the neutron star mass. The lighter neutron stars have a lower average density and a lower ν_{K} , making them have higher reduced frequencies than the massive ones.

Since the Kepler frequency is EOS dependent (see, e.g., Li et al. 2016, 2017), the reduced frequencies thus obtain a more complicated EOS dependence. With the rigid crust, as shown in Eqs. (7)-(8), the location R_c of the crust-core transition plays an important role. In this case, the strong EOS dependence of R_c makes the reduced frequency more strongly EOS dependent than the case with an elastic crust. While in the latter case, both the ν_{crit} and ν_{K} are calculated by integrating from the center to the surface. The reduced frequency obtained appears rather EOS insensitive due to some canceling effects in taking the ratio. Finally, the difference in the reduced frequency between the two cases at the same temperature are very large. More quantitatively, for a typical temperature $T = 10^8$ K relevant for the LMXBs, ν_{crit} is lifted from $\sim 0.16 \nu_{\text{K}}$ ($\sim 0.13 \nu_{\text{K}}$) to $\sim 0.79 \nu_{\text{K}}$ ($\sim 0.48 \nu_{\text{K}}$) for $M = 1.4 M_{\odot}$ ($M = 2.0 M_{\odot}$)

Table 1. Neutron star properties based on the 5 unified EOSs models (Fortin et al. 2016). M_{TOV} is the maximum mass of non-rotating neutron stars supported by the given EOS. ν_{min} is the minimum frequency (in unit of the Kepler frequency ν_{K}) to support GW190814’s secondary component m_2 with a minimum mass of $2.50 M_{\odot}$. T_{max} is the maximum temperature for the m_2 to remain r-mode stable.

Model	M_{TOV} (M_{\odot})	ν_{K} (Hz)	ν_{min} (ν_{K})	T_{max} (K)
DD2	2.42	1196.6	0.755	3.0×10^7
DDME2	2.48	1169.6	0.744	3.9×10^7
SKb	2.20	1446.5	0.809	1.3×10^7
SkI6	2.20	1433.4	0.827	1.1×10^7
SLy9	2.16	1515.4	0.855	7.5×10^6

neutron stars when assuming a rigid crust with respect to the elastic one.

In short, the main lessons we learned from this section that are most important for our following study about the r-mode stability of m_2 are (1) the rigid crust provides the strongest damping, (2) the stability of the 19 neutron stars in LMXBs favors the rigid crust damping, (3) the reduced critical frequency $\nu_{\text{crit}}/\nu_{\text{K}}$ with the rigid crust is sensitive to both the neutron star mass and the EOS used.

4. R-MODE STABILITY OF GW190814’S SECONDARY COMPONENT OF MASS $2.50 M_{\odot}$

We now turn to examine the r-mode stability of GW190814’s secondary component m_2 as a super-massive and superfast pulsar. For this purpose, we first find the minimum frequency ν_{min} to support GW190814’s secondary component with a minimum mass of $2.50 M_{\odot}$ (Abbott et al. 2020) using the well-tested RNS code (Stergioulas et al. 1995) for a given EOS. Among the 6 EOSs used above, we found that the SLy2 EOS can not rotationally support a $2.50 M_{\odot}$ star even at the Kepler frequency. Thus, only the remaining 5 EOSs are used. As discussed in the previous section, only the damping with the rigid crust is necessary for this discussion as it provides the strongest/quickest damping.

Listed in Table 1 are the maximum mass of non-rotating neutron stars M_{TOV} , Kepler frequency ν_{K} and the minimum frequency ν_{min} to support a neutron star of mass $2.50 M_{\odot}$ for the 5 EOSs used. The ν_{min} is then plotted as a horizontal line in Fig. 5 where the r-mode stability boundary for each EOS is shown in the frequency-temperature plane. Their cross point is marked with a diamond indicating the maximum temperatures T_{max} below which neutron stars remain r-

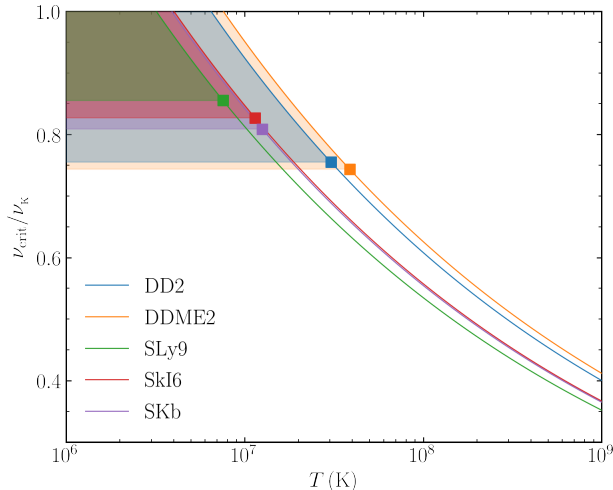


Figure 5. Temperature dependence of the reduced critical frequency $\nu_{\text{crit}}/\nu_{\text{K}}$ for neutron stars with rigid crusts. For each EOS, the $\nu - T$ space allowing the secondary component of GW190814 as a r-mode stable pulsar is shown as the shaded region. The maximum temperatures T_{max} below which neutron stars remain r-mode stable are marked with diamonds on the r-mode instability thresholds for the 5 EOSs used.

mode stable. The resulting 5 maximum temperatures are listed in the last column in Table 1. While the allowed $\nu - T$ parameter spaces are reported with the shaded regions in Fig. 5.

As expected, the ν_{min} depends sensitively on the M_{TOV} determined by the stiffness of the EOS. For the 5 EOSs used, the ν_{min} and M_{TOV} range between 0.744 to $0.855 \nu_{\text{K}}$ and 2.16 to $2.42 M_{\odot}$, respectively. The corresponding maximum temperature T_{max} is between 7.5×10^6 to 3.9×10^7 K. This temperature limit is about 10 times cooler than the LMXBs but also about 10 times hotter than some of the known old neutron stars (Wijnngaarden et al. 2019). This information may be useful for further understanding the dynamical path of the GW190814 event and the nature of its secondary component.

The required minimum frequencies ν_{min} between 870 Hz and 1295 Hz found here with the 5 selected EOSs satisfying all currently known constraints from both nuclear physics and astrophysics cover the minimum frequencies found necessary for the m_2 to rotationally sustain a minimum mass of $2.50 M_{\odot}$ in Most et al. (2020); Zhang & Li (2020); Biswas et al. (2020). As discussed above, as long as the m_2 has a temperature below about 3.9×10^7 K, the m_2 spinning with the high frequencies found above can remain r-mode stable. While it is not the purpose of this work to study how the high mass and spin can be obtained, it is very interesting to note

that it was already pointed out by Safarzadeh & Loeb (2020) that they could be supplied through the circumbinary accretion disk if the m_2 was born as a neutron star where a significant amount of the supernova ejecta mass from its formation remained bound to the binary due to the presence of the massive black hole companion in the GW190814 event.

5. CONCLUSIONS

In conclusion, the GW190814’s secondary component m_2 can be an r-mode stable supermassive and superfast pulsar rotating with a frequency higher than 870.2 Hz (0.744 times its Kepler frequency of 1169.6 Hz) as long as its temperature is lower than about 3.9×10^7 K which is still about 10 times hotter than some of the known old neutron stars. Thus, the r-mode instability should not be a concern for the m_2 . The minimum frequency and limiting temperature found here may be useful for further understanding the formation mechanism of m_2 and the merger dynamics of GW190814.

Our study is carried out within the minimum model of neutron stars consisting of only nucleons and leptons. Moreover, the fast rotation is probably the simplest mechanism to provide the additional support besides the nuclear pressure against the strong gravity of massive neutron stars. Furthermore, we selected the EOSs satisfying all currently known astrophysical and nuclear physics constraints from a group of 33 unified EOSs constructed from the crust to the core consistently using the same nuclear interactions. Thus, our approach is probably among the most conservative ones used in the literature in investigating the nature of GW190814’s secondary component.

A major caveat of our work is the assumption that the rigid crust of neutron stars provides the strongest r-mode damping among a multitude of possible damping mechanisms. While both our current work and previous theoretical calculations by others as well as the stability of the 19 neutron stars in LMXBs favor the dominating rigid crust damping, there may be other even stronger damping mechanisms and/or model ingredients affecting significantly the location of the r-mode instability windows. Nevertheless, our current study can successfully describe all relevant observations of neutron stars. We are thus confident that our present conclusions are physically sound and useful for the community to finally solve the mystery regarding the nature of GW190814’s secondary component.

ACKNOWLEDGMENTS

We would like to thank Morgane Fortin for valuable discussions. This work is supported in part by National SKA Program of China (No. 2020SKA0120300), the National Natural Science Foundation of China (Grant Nos. 11873040, 12033001), the Youth Innovation Fund of Xiamen (No. 3502Z20206061), the CAS “Light of West China” Program (No. 2019-XBQNXZ-B-016), the Tianshan Youth Program (No. 2018Q039), the U.S. Department of Energy, Office of Science, under Award Number DE-SC0013702, the CUSTIPEN (China-U.S. Theory Institute for Physics with Exotic Nuclei) under the US Department of Energy Grant No. DE-SC0009971.

REFERENCES

- Abbott, R., Abbott, T. D., Abraham, S., et al. 2020, *ApJL*, 896, L44. doi:10.3847/2041-8213/ab960f
- Alford, M. G. & Schwenzer, K. 2014, *NuPhA*, 931, 740. doi:10.1016/j.nuclphysa.2014.08.077
- Alford, M. G. & Schwenzer, K. 2014, *PhRvL*, 113, 251102. doi:10.1103/PhysRevLett.113.251102
- Andersson, N. & Kokkotas, K. D. 1998, *MNRAS*, 299, 1059. doi:10.1046/j.1365-8711.1998.01840.x
- Andersson, N. 1998, *ApJ*, 502, 708. doi:10.1086/305919
- Andersson, N. & Kokkotas, K. D. 2001, *International Journal of Modern Physics D*, 10, 381. doi:10.1142/S0218271801001062
- Andersson, N., Haskell, B., & Comer, G. L. 2010, *PhRvD*, 82, 023007. doi:10.1103/PhysRevD.82.023007
- Andersson, N. 2017, *Journal of Astrophysics and Astronomy*, 38, 58. doi:10.1007/s12036-017-9463-8
- Baldo, M. & Burgio, G. F. 2016, *Progress in Particle and Nuclear Physics*, 91, 203. doi:10.1016/j.ppnp.2016.06.006
- Biswas, B., Nandi, R., Char, P., et al. 2020, arXiv:2010.02090
- Bombaci, I., Drago, A., Logoteta, D., et al. 2020, arXiv:2010.01509
- Chandrasekhar, S. 1970, *PhRvL*, 24, 611. doi:10.1103/PhysRevLett.24.611
- Chugunov, A. I., Gusakov, M. E., & Kantor, E. M. 2017, *MNRAS*, 468, 291. doi:10.1093/mnras/stx391
- Cromartie, H. T., Fonseca, E., Ransom, S. M., et al. 2020, *Nature Astronomy*, 4, 72. doi:10.1038/s41550-019-0880-2
- Cutler, C. & Lindblom, L. 1987, *ApJ*, 314, 234. doi:10.1086/165052
- Dai, Z. G., Wang, S. Q., Wang, J. S., et al. 2016, *ApJ*, 817, 132. doi:10.3847/0004-637X/817/2/132
- Dexheimer, V., Gomes, R. O., Klähn, T., et al. 2020, arXiv:2007.08493
- Flowers, E. & Itoh, N. 1979, *ApJ*, 230, 847. doi:10.1086/157145
- Fortin, M., Providência, C., Raduta, A. R., et al. 2016, *PhRvC*, 94, 035804. doi:10.1103/PhysRevC.94.035804
- Friedman, J. L. & Schutz, B. F. 1978, *ApJ*, 222, 281. doi:10.1086/156143
- Friedman, J. L. & Morsink, S. M. 1998, *ApJ*, 502, 714. doi:10.1086/305920
- Glampedakis, K. & Andersson, N. 2006, *PhRvD*, 74, 044040. doi:10.1103/PhysRevD.74.044040
- Godzieba, D. A., Radice, D., & Bernuzzi, S. 2020, arXiv:2007.10999
- Gusakov, M. E., Chugunov, A. I., & Kantor, E. M. 2014, *PhRvD*, 90, 063001. doi:10.1103/PhysRevD.90.063001
- Haskell, B. & Andersson, N. 2010, *MNRAS*, 408, 1897. doi:10.1111/j.1365-2966.2010.17255.x
- Haskell, B., Degenaar, N., & Ho, W. C. G. 2012, *MNRAS*, 424, 93. doi:10.1111/j.1365-2966.2012.21171.x
- Haskell, B. 2015, *International Journal of Modern Physics E*, 24, 1541007. doi:10.1142/S0218301315410074
- Hessels, J. W. T., Ransom, S. M., Stairs, I. H., et al. 2006, *Science*, 311, 1901. doi:10.1126/science.1123430
- Ho, W. C. G. & Lai, D. 2000, *ApJ*, 543, 386. doi:10.1086/317085
- Ho, W. C. G., Andersson, N., & Haskell, B. 2011, *PhRvL*, 107, 101101. doi:10.1103/PhysRevLett.107.101101
- Huang, K., Hu, J., Zhang, Y., et al. 2020, arXiv:2008.04491
- Idrisy, A., Owen, B. J., & Jones, D. I. 2015, *PhRvD*, 91, 024001. doi:10.1103/PhysRevD.91.024001
- Kokkotas, K. D. & Schwenzer, K. 2016, *European Physical Journal A*, 52, 38. doi:10.1140/epja/i2016-16038-9
- Krüger, C. J. & Kokkotas, K. D. 2020, *PhRvL*, 125, 111106. doi:10.1103/PhysRevLett.125.111106

- Lattimer, J. M., Pethick, C. J., Prakash, M., et al. 1991, *PhRvL*, 66, 2701. doi:10.1103/PhysRevLett.66.2701
- Lattimer, J. M. & Prakash, M. 2000, *PhR*, 333, 121. doi:10.1016/S0370-1573(00)00019-3
- Li, A., Zhang, B., Zhang, N.-B., et al. 2016, *PhRvD*, 94, 083010. doi:10.1103/PhysRevD.94.083010
- Li, A., Zhu, Z.-Y., & Zhou, X. 2017, *ApJ*, 844, 41. doi:10.3847/1538-4357/aa7a00
- Li, A., Zhu, Z.-Y., Zhou, E.-P., et al. 2020, arXiv:2007.05116
- Li, B.-A. & Han, X. 2013, *Physics Letters B*, 727, 276. doi:10.1016/j.physletb.2013.10.006
- Li, B.-A., Ramos, À., Verde, G., et al. 2014, *European Physical Journal A*, 50, 9. doi:10.1140/epja/i2014-14009-x
- Li, B.-A., Krastev, P. G., Wen, D.-H., et al. 2019, *European Physical Journal A*, 55, 117. doi:10.1140/epja/i2019-12780-8
- Li, B.-A. & Magno, M. 2020, *PhRvC*, 102, 045807. doi:10.1103/PhysRevC.102.045807
- Lindblom, L., Owen, B. J., & Morsink, S. M. 1998, *PhRvL*, 80, 4843. doi:10.1103/PhysRevLett.80.4843
- Lindblom, L., Owen, B. J., & Ushomirsky, G. 2000, *PhRvD*, 62, 084030. doi:10.1103/PhysRevD.62.084030
- Madsen, J. 2000, *PhRvL*, 85, 10. doi:10.1103/PhysRevLett.85.10
- Miller, M. C., Lamb, F. K., Dittmann, A. J., et al. 2019, *ApJL*, 887, L24. doi:10.3847/2041-8213/ab50c5
- Most, E. R., Papenfort, L. J., Weih, L. R., et al. 2020, *MNRAS*, 499, L82. doi:10.1093/mnras/laa168
- Moustakidis, C. C. 2015, *PhRvC*, 91, 035804. doi:10.1103/PhysRevC.91.035804
- Newton, W. G. & Crocombe, G. 2020, arXiv:2008.00042
- Oertel, M., Hempel, M., Klähn, T., et al. 2017, *Reviews of Modern Physics*, 89, 015007. doi:10.1103/RevModPhys.89.015007
- Ofengeim, D. D., Gusakov, M. E., Haensel, P., et al. 2019, *PhRvD*, 100, 103017. doi:10.1103/PhysRevD.100.103017
- Papazoglou, M. C. & Moustakidis, C. C. 2016, *Ap&SS*, 361, 98. doi:10.1007/s10509-016-2692-5
- Providência, C., Fortin, M., Pais, H., et al. 2019, *Frontiers in Astronomy and Space Sciences*, 6, 13. doi:10.3389/fspas.2019.00013
- Raaijmakers, G., Riley, T. E., Watts, A. L., et al. 2019, *ApJL*, 887, L22. doi:10.3847/2041-8213/ab451a
- Rieutord, M. 2001, *ApJ*, 550, 443. doi:10.1086/319705
- Riley, T. E., Watts, A. L., Bogdanov, S., et al. 2019, *ApJL*, 887, L21. doi:10.3847/2041-8213/ab481c
- Roupas, Z., Panotopoulos, G., & Lopes, I. 2020, arXiv:2010.11020
- Sá, P. M. 2004, *PhRvD*, 69, 084001. doi:10.1103/PhysRevD.69.084001
- Sá, P. M. & Tomé, B. 2005, *PhRvD*, 71, 044007. doi:10.1103/PhysRevD.71.044007
- Safarzadeh, M. & Loeb, A. 2020, *ApJL*, 899, L15. doi:10.3847/2041-8213/aba9df
- Shternin, P. S. & Yakovlev, D. G. 2008, *PhRvD*, 78, 063006. doi:10.1103/PhysRevD.78.063006
- Steiner, A. W., Prakash, M., Lattimer, J. M., et al. 2005, *PhR*, 411, 325. doi:10.1016/j.physrep.2005.02.004
- Stergioulas, N. et al., 1995, RNS code, <http://www.gravity.phys.uwm.edu/rns/>
- Tews, I., Pang, P. T. H., Dietrich, T., et al. 2020, arXiv:2007.06057
- Vidaña, I., Providência, C., Polls, A., et al. 2009, *PhRvC*, 80, 045806. doi:10.1103/PhysRevC.80.045806
- Vidaña, I. 2012, *PhRvC*, 85, 045808. doi:10.1103/PhysRevC.85.045808
- Wang, Y.-B., Zhou, X., Wang, N., et al. 2019, *Research in Astronomy and Astrophysics*, 19, 030. doi:10.1088/1674-4527/19/2/30
- Wen, D.-H., Newton, W. G., & Li, B.-A. 2012, *PhRvC*, 85, 025801. doi:10.1103/PhysRevC.85.025801
- Wijngaarden, M. J. P., Ho, W. C. G., Chang, P., et al. 2019, *MNRAS*, 484, 974. doi:10.1093/mnras/stz042
- Xie, W.-J. & Li, B.-A. 2020, *ApJ*, 899, 4. doi:10.3847/1538-4357/aba271
- Xu, J., Chen, L.-W., Li, B.-A., et al. 2009, *ApJ*, 697, 1549. doi:10.1088/0004-637X/697/2/1549
- Yang, S.-H., Pi, C.-M., & Zheng, X.-P. 2011, *ApJL*, 735, L29. doi:10.1088/2041-8205/735/2/L29
- Zhang, N.-B., Li, B.-A., & Xu, J. 2018, *ApJ*, 859, 90. doi:10.3847/1538-4357/aac027
- Zhang, C. & Mann, R. B. 2020, arXiv:2009.07182
- Zhang, N.-B. & Li, B.-A. 2019, *European Physical Journal A*, 55, 39. doi:10.1140/epja/i2019-12700-0
- Zhang, N.-B. & Li, B.-A. 2020, *ApJ*, 902, 38. doi:10.3847/1538-4357/abb470